Manipulating Deformable Objects with a Dual-arm Robot

Stéphane Caro[1] [a], Christine Chevallereau[1] [b] and Alberto Remus[2]

[1]*Centre National de la Recherche Scientifique (CNRS), Laboratoire des Sciences du Numérique de Nantes (LS2N),*
44300 Nantes, France
[2]*École Centrale de Nantes, 44300 Nantes, France*

Keywords: Deformable Models, Dual-arm Robot, Manipulation, Stability Analysis.

Abstract: Competition in all sectors requires companies to be increasingly flexible to market changes and the assembly industry is no exception. The impact of this work concerns aircraft production, as well as other fields. The main focus is on modelling and control techniques to carry out assembly tasks involving deformable parts, by exploiting a multi-robot system. Specifically, two robot arms are used to move a light and deformable part in order to adapt its shape for an assembly operation. A vision system is used, assisted by markers. Furthermore, the stability of the proposed controller is analyzed and experimental results are given.

1 INTRODUCTION

Assembly process is one of the cornerstones of industry because it allows to couple parts together in order to get a sub-product or a finished product (Marvel *et al.* (2018)). This work investigates the added value brought by a robotic system composed by robots, which have to cooperate in order to perform an assembly task involving deformable objects. Manipulation of flexible objects has been considered in prior work with different control approaches such as impedance control (Sun and Liu (1997)) and (Erhart and Hirche (2013)), force control (Sun and Liu (2001)) or sliding mode control (Tavasoli *et al.* (2009)). Visual approaches have also been used in several studies (Smolen and Patriciu (2009)), (Hirai and Wada (2000)),(Wada *et al.* (2001)) using a theoretical model of the object deformation or with an adaptive model of deformation built online (Navarro-Alarcon *et al.* (2016)). Here a visual approach is investigated as well, but a constant model of the beam deformation is used since the results of stability analysis show that an adaptive model is not required to manipulate the object at hand. Several papers are dedicated to more compliant objects such as tissues (Berenson (2013); Jia *et al.* (2018)). Under some assumptions, many parts to be assembled in industry can be modelled as planar flexible beams (Bertelsmeier *et al.* (2017)) and this greatly

simplifies the modelling and control, which is common in industry like aircraft production (Al-Yahmadi and Hsia (2007)). To reproduce an assembly task, the work cell used in the framework of this research work is endowed with a fixture coupled to a flexible beam. A new modelling technique is presented based on the elastic properties of the beam, which can be exploited to measure its deformation. The control aspect and the use of vision are essential because of the uncertainties in the flexible object modelling (Navarro-Alarcon *et al.* (2016)).

Several robots cooperating and manipulating the same object amount to a closed-loop mechanism with a deformable beam. Such a system is under-actuated due the infinite number of degrees of freedom induced by the flexible beam. Here some key points are located on the beam to ease the control of the overall system. Contrary to methods that use a physical model of the deformable object and its stable equilibrium (Bretl and McCarthy (2014)),(Sintov *et al.* (2020)), very simple deformation models adapted to our control strategy will be used. Moreover, this first-order model can be built experimentally based on visual information.

The main contribution of this paper, essentially methodological, lies in the use of the model estimation for the motion control of a deformable beam and the stability analysis of the proposed controlled law. It should be noted that the proposed approach is based on a classical position control available on all industrial robots, and a high level loop based on vision

feedback. The approach does not require force measurement or force control. Besides, it is simpler than the one introduced in (Navarro-Alarcon *et al.* (2016)) because it is based on a non-adaptive model and defined from the desired object pose thanks to a detailed stability analysis. Furthermore, it is well suited to industrial applications and manipulation of large objects, but less flexible than those considered in (Navarro-Alarcon *et al.* (2016)) and (Lagneau *et al.* (2020)).

The paper is organized as follows. Section 2 presents the experimental setup and its parameterization. Section 3 introduces the kinematic sensitivity Jacobian matrix associated with the beam shaping and displacement in a plane. Section 4 describes the proposed control law of the dual-arm robot and its performance in terms of stability and accuracy. Finally, conclusions are drawn in Section 5.

2 EXPERIMENTAL SETUP

The section describes the robotic cell and its main components used in the framework of the research work presented in the paper. Besides, a simplified model of the multi-robot system and the four spaces at stake used for its control are explained.

As shown in Figs. 1 and 2, the experimental setup located at LS2N is composed of (*i*) two KUKA LWR 4+ 7-dof robotic arms, the left one being endowed with a two-fingers gripper and the right one being equipped with a three-fingers hand; (*ii*) one flexible beam; (*iii*) one target, named *target shape*, for the beam; (*iv*) one ®Logitech C905 camera, which is used as a detection system to extract keypoints from both the beam and the target shape.
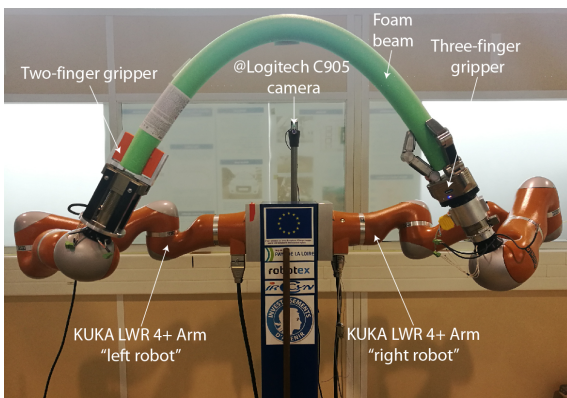

Figure 1: A flexible beam grasped by two KUKA LWR 4+ 7-dof robotic arms.

The two robots are position-based controlled. Contrary to the geometric and kinematic models of the robots, the model of the flexible beam is not known beforehand. Therefore, a technique to obtain this model is described in this paper based on some *ArUco Markers* (Garrido-Jurado *et al.* (2014)) stuck on the beam as illustrated in Fig. 3. The shape and

Figure 2: Target shape for the flexible beam.

position of the target shape are supposed to be still in the workcell. Note that the flexible beam is initially positioned by a human operator, due to the complexity of the automatic detection and grasping of the flexible beam.
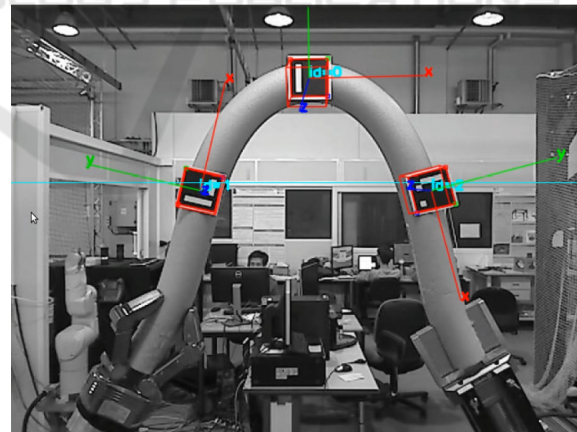

Figure 3: Three ArUco Markers stuck on the flexible beam and detected by a ®Logitech C905 camera through OpenCV.

2.1 The Multi-robot System

The two serial robots and the flexible beam can be seen as a planar closed-loop mechanism, which is intrinsically under-actuated due to the infinite number

of degrees of freedom provided by the flexible beam as depicted in Fig. 4. Without loss of generality, the beam and its attachement points E_l and E_r with the grippers are supposed to move in the plane passing through point O and normal to x_b, x_b being normal to both axes y_b and z_b. Thus, the beam does not twist during its positioning and shaping in the base frame $\mathcal{F}_b$ of origin O and axes y_b and z_b. The planar displacement of the left (right, resp.) robot is parameterized by the Cartesian coordinates y_l and z_l (y_r and z_r, resp.) of point E_l (E_r, resp.) expressed in $\mathcal{F}_b$.
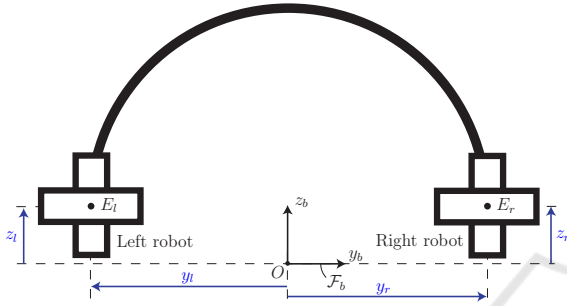

Figure 4: Planar closed-loop mechanism composed of a flexible beam and two grippers.

The robots are assumed to behave like rigid systems with regard to the beam, the latter being much more flexible. As a consequence, variables y_l, z_l, y_r and z_r should be controlled to position and shape the flexible beam in order to superimpose it the target shape for the beam shown in Fig. 2. Therefore, a modelling and control strategy of the flexible beam should first be developed based on the location of the ArUco Markers expressed in $\mathcal{F}_b$ and detected by the ®Logitech C905 camera.

2.2 Four Spaces

In order to reach its target shape shown in Fig. 2, the flexible beam is deformed and displaced by the two KUKA LWR 4+ 7-dof robotic arms, named left and right robots respectively in what remains, endowed with their own gripper as shown in Fig.1. It is noteworthy that four spaces are at stake to deform and move the beam in $\mathcal{F}_b$. Those four spaces are defined as follows: (*i*) the robots joint space ($\mathcal{RJS}$) is the set of robot revolute joint variables, namely,

$$\mathcal{RJS} = \{\mathbf{q} = [\dots q_{ij} \dots]^T \in \mathbb{R}^{14} : \underline{q}_{ij} \leq q_{ij} \leq \overline{q}_{ij},$$
$$i = l, r, \, j = 1, \dots, 7\} \quad (1)$$

$\underline{q}_{ij}$ and $\overline{q}_{ij}$ being the lower and upper bounds of revolute joint angle q_{ij} and are given in [1]. l and r

[1]https://www.kuka.com/en-de/products/robot-systems/industrial-robots/lbr-iiwa

stand for the left and right robots, resp.; (*ii*) the end-effector space ($\mathcal{EES}$) is the set Cartesian coordinates of points E_l and E_r expressed in $\mathcal{F}_b$ satisfying the planar closed-loop shown in Fig. 4, namely,

$$\mathcal{EES} = \{\mathbf{p} = [y_l \, z_l \, y_r \, z_r]^T \in \mathbb{R}^4 :$$
$$(y_r - y_l)^2 + (z_r - z_l)^2 \leq l_b^2\} \quad (2)$$

l_b being the length of the flexible beam; (*iii*) the deformation input space ($\mathcal{DIS}$) is the set of variables associated to the positioning and shaping of the beam:

$$\mathcal{DIS} = \{\mathbf{u} = [y_d \, z_d \, y_m \, z_m]^T \in \mathbb{R}^4 : \text{(5a)-(d) are satisfied}\} \quad (3)$$

variables y_d, z_d, y_m, z_m being depicted in Fig. 5; (*iv*) the keypoint space ($\mathcal{KS}$) defines the location of the ArUco Markers stuck on the flexible beam, i.e.,

$$\mathcal{KS} = \{\mathbf{x} = [y_1 \, z_1 \dots y_N \, z_N]^T \in \mathbb{R}^{2N}\} \quad (4)$$

y_k and z_k being the Cartesian coordinates of keypoint P_k expressed in $\mathcal{F}_b$, $k = 1, \dots, N$ with N the number of keypoints as shown in Fig. 5.
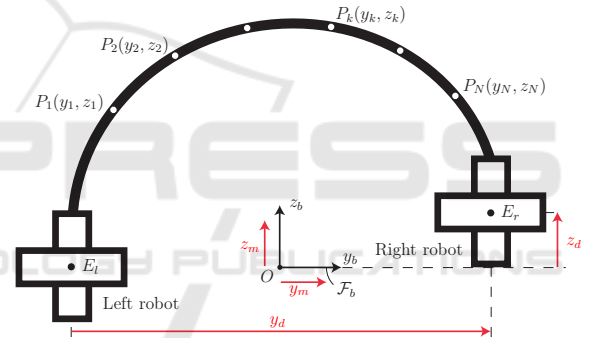

Figure 5: Variables associated with $\mathcal{DIS}$ and $\mathcal{KS}$.

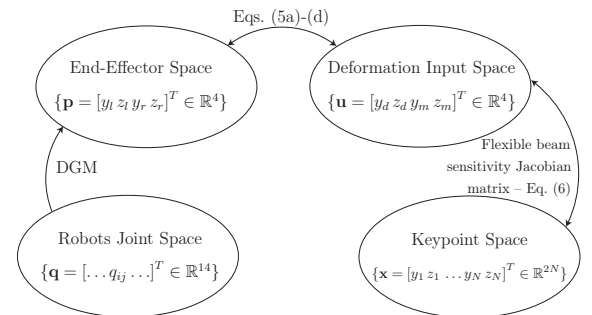The relationships between the four spaces are represented in Fig. 6.

Figure 6: Relationship between the robots joint, end-effector, deformation input and keypoint spaces.

3 BEAM DEFORMATION

The beam is displaced and shaped by controlling the overall system in $\mathcal{DIS}$. From Figs. 4 and 5, the variables y_m, z_m devoted to the positioning of the beam in $\mathcal{F}_b$ and the variables y_d, z_d related to its shaping are defined as a function of Cartesian coordinates of points E_l and E_r as follows:

$$y_d = y_l - y_r \tag{5a}$$
$$z_d = z_l - z_r \tag{5b}$$
$$y_m = (y_l + y_r)/2 \tag{5c}$$
$$z_m = (z_l + z_r)/2 \tag{5d}$$

It should be noted that the precision of the beam modeling from the keypoint detection is a function of N. The higher N, the better the precision. The maximum number of keypoints to avoid an under-actuated system is two. Indeed, if $N = 2$, the system will have as many input variables as ouput variables. On the contrary, the number of input variables is lower than the number of output variables, i.e., $2N$, when $N > 2$. Figure 7 shows an example of a simulated under-actuated system where with three keypoints are located both on the beam and its target shape. Note that each keypoint on the beam is assigned to its own keypoint on the target shape.
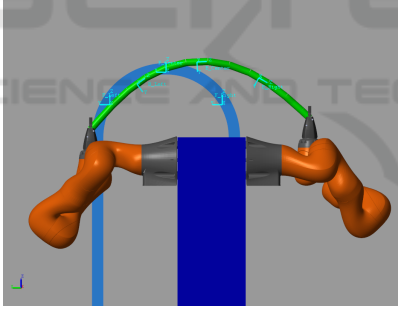

Figure 7: Three keypoints located both on the beam and its target shape: the system is under-actuated.

3.1 Sensitivity Matrix

The variation $\delta\mathbf{x}$ in keypoint vector $\mathbf{x}$, defined in (4), can be expressed as a function of the variation $\delta\mathbf{u}$ in input variable vector $\mathbf{u}$, defined in (3), as follows:

$$\delta\mathbf{x} = \mathbf{J}(y_d, z_d)\,\delta\mathbf{u} \tag{6}$$

where $\mathbf{J}$ is a $(2N \times 4)$-sensitivity Jacobian matrix, as in (Caro $et\ al.$ (2009)), taking the form:

$$\mathbf{J} = \begin{bmatrix} \mathbf{j}_{yd} & \mathbf{j}_{zd} & \mathbf{j}_{ym} & \mathbf{j}_{zm} \end{bmatrix} \tag{7}$$

δy_m and δz_m correspond to a small displacement of the whole beam, thus they affect the displacement of all the keypoints with the same manner. However, they do not affect the shape of the beam. Thus, the last two columns $\mathbf{j}_{ym}$ and $\mathbf{j}_{zm}$ of matrix $\mathbf{J}$ are expressed as:

$$\mathbf{j}_{ym} = \begin{bmatrix} 1 & 0 & 1 & 0 & \dots & 1 & 0 \end{bmatrix}^T \tag{8}$$
$$\mathbf{j}_{zm} = \begin{bmatrix} 0 & 1 & 0 & 1 & \dots & 0 & 1 \end{bmatrix}^T \tag{9}$$

$\mathbf{j}_{yd}$ and $\mathbf{j}_{zd}$ are the first two columns of matrix $\mathbf{J}$ and two $2N$-dimensional vectors taking the form:

$$\mathbf{j}_{yd} = \begin{bmatrix} \dots & \delta y_k/\delta y_d & \delta z_k/\delta y_d & \dots \end{bmatrix}^T \tag{10}$$
$$\mathbf{j}_{zd} = \begin{bmatrix} \dots & \delta y_k/\delta z_d & \delta z_k/\delta z_d & \dots \end{bmatrix}^T \tag{11}$$

with $k = 1, \dots, N$. $\delta y_k/\delta y_d$ ($\delta z_k/\delta y_d$, resp.) denotes the sensitivity of coordinate y_k (z_k, resp.) to variation δy_d in variable y_d. $\delta y_k/\delta z_d$ ($\delta z_k/\delta z_d$, resp.) denotes the sensitivity of coordinate y_k (z_k, resp.) to variation δz_d in variable z_d. Those sensitivity coefficients are not a function of variables y_m and z_m.

The terms of the first two column vectors $\mathbf{j}_{yd}$ and $\mathbf{j}_{zd}$ of matrix $\mathbf{J}$ are identified either in simulation as explained in Sec. 3.2 or experimentally as described in Sec. 3.3 for a given shape of the beam, i.e., for given y_d and z_d nominal values. The identification methodology aims at measuring the point-displacements of keypoints P_k, $k = 1, \dots, N$, namely, the variations δy_k and δz_k in their Cartesian coordinates for several small variations δy_d and δz_d.

3.2 Simulation

The robotic platform shown in Fig. 1 was simulated thanks to Simscape Multibody$^{\text{TM}}$ and Simulink$^{\text{TM}}$ to deal with modelling, control and visualization. The beam was modeled based on the lumped parameters method presented in (Miller $et\ al.$ (2006)). The beam was discretized in twelve mass unit, linked together by revolutes joint endowed with a certain stiffness and damping, whose parameters depend on the material used. As far as the foam beam depicted in Fig. 1 is concerned, its length l_b and diameter d_b are equal to 1.14 m and 0.064 m, respectively. The Young's modulus E and density ρ of the foam are equal to 0.005 GPa and 50 kg/m^3, respectively.

In what remains, three keypoints are supposed to be equally spaced on the beam, i.e. $N = 3$, to match with the three ArUco Markers shown in Fig. 3.

Figure 8 shows the variations δz_1, δz_2 and δz_3 in the z-coordinates of points P_1, P_2 and P_3 associated with small variations δy_d as a function of y_d, y_d varying from 0.8 m to 1 m. It is apparent that the higher y_d, i.e., the larger the distance points E_l and E_r, the more sensitive the z-coordinates of the keypoints to small variations in y_d. Besides, the z-coordinate of the mid-keypoint P_2 is more sensitive to δy_d than the z-coordinates of the lateral keypoints P_1 and P_3. The

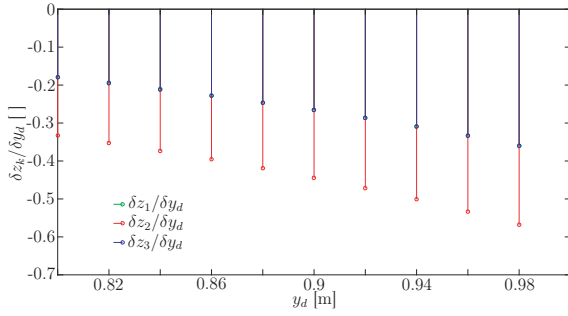plots corresponding to P_1 and P_3 overlap because the last two keypoints have the same sensitivity to δy_d.

Figure 8: Sensitivity of the z-coordinates of keypoints P_1, P_2 and P_3 to small variations in y_d obtained from simulation.
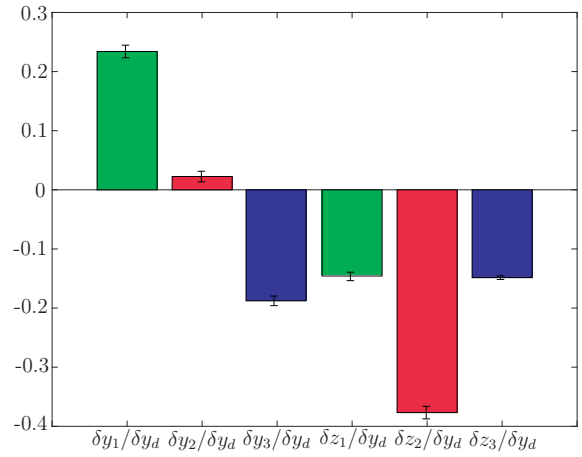
3.3 Experiments

As explained in Sec. 3.1, the terms of matrix $\mathbf{J}$ can also be identified experimentally. Experiments were carried out by gluing three ArUco Markers on the foam beam as illustrated in Fig. 3 and by using a calibrated monocular camera to detect them. Robot Operating System was used to control the robots.

Twenty tests were performed per set of y_d and z_d nominal values to determine the mean and standard deviation of the sensitivity coefficients $\delta y_k/\delta y_d$, $\delta z_k/\delta y_d$, $\delta y_k/\delta z_d$ and $\delta z_k/\delta z_d$, $k = 1, 2, 3$. Figure 9 highlights the mean values of those coefficients for $y_d = 0.8$ m and $z_d = 0$ m. Furthermore, Fig. 9 shows the confidence intervals associated with the foregoing sensitivity coefficients and assessed experimentally by considering the following sources of errors: (*i*) camera calibration and placement errors; (*ii*) uncertainties in the beam grasping; (*iii*) bad knowledge of the beam characteristics; (*iv*) vibrations of the keypoints and slight scattering during trajectory execution.

It should be noted that the sensitiviy coefficients identified experimentally differ slightly from the simulation results shown in Fig. 8. More confidence can be given to experimental results because the confidence intervals are quite small and the uncertainties in the experimental setup and in the flexible beam model are difficult to take into account in simulation.

4 CONTROL LAW

The objective of the control law is to bring the ArUco Markers, i.e. the keypoints, stuck on the flexible beam, as shown in Fig. 3, in front of the markers glued on the target shape illustrated in Fig. 2. The closed loop control law that defines the displacement of end-

(a)
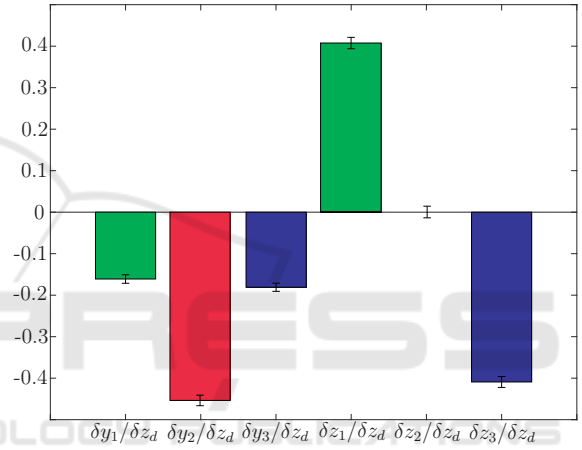
(b)

Figure 9: Experimental mean values and confidence intervals associated with the terms of (a) $\mathbf{j}_{yd}$ and (b) $\mathbf{j}_{zd}$ for $y_d = 0.8$ m and $z_d = 0$ m.

effectors E_l and E_r in $\mathcal{DIS}$ is described in this section. Then classical control of the robot is used with a low level control in $\mathcal{RJS}$ as shown in Fig. 10.
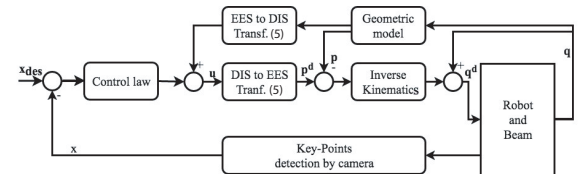

Figure 10: Overall control scheme for position and shape control.

The desired end-effector pose vector $\mathbf{p}$ is expressed from the deformation input vector $\mathbf{u}$ by Eqs. (5a)-(d). Note that the KUKA LWR 4+ robotic arm is kinematically redundant because it has seven revolute joints. Therefore, the Moore-Penrose inverse of the kinematic Jacobian matrix of each robotics

arm is used to compute $\delta\mathbf{q}$, the variation in revolute joint angle vector $\mathbf{q}$ as a function of a small displacement $\delta\mathbf{p}$ of end-effectors E_l and E_r in $\mathcal{F}_b$. Then the desired revolute joint angle vector $\mathbf{q}$ is deduced and sent to the low level controller of the robot.

The control law used to define vector $\mathbf{u}$ is based on visual servoing control in the task space (Chaumette *et al.* (1991)). It should be noted that the sensitivity Jacobian matrix (7) amounts to an *interaction matrix*. From Eq. (7), the end-effector velocity $\dot{\mathbf{x}}$ is expressed as a function of the time derivative $\dot{\mathbf{u}}$ of vector $\mathbf{u}$ as follows:

$$\dot{\mathbf{x}} = \mathbf{J}\dot{\mathbf{u}} \qquad (12)$$

with $\mathbf{x}$ being defined in (4). Let $\mathbf{x}_{des}$ denote the desired keypoints coordinate vector expressed in $\mathcal{F}_b$. Thus, the error $\mathbf{e}$ in $\mathcal{KS}$ takes the form:

$$\mathbf{e} = \mathbf{x} - \mathbf{x}_{des} \qquad (13)$$

The following equation should be met for $\mathbf{e}$ to decrease with an exponential rate:

$$\dot{\mathbf{e}} = -\lambda\mathbf{e} \qquad (14)$$

with λ being a positive gain and $\dot{\mathbf{e}}$ the time derivative of $\mathbf{e}$. By substituting (13) into (14) and assuming that $\mathbf{x}_{des}$ is constant, we get:

$$\dot{\mathbf{x}} = -\lambda(\mathbf{x} - \mathbf{x}_{des}) \qquad (15)$$

Since the relation between $\mathbf{x}$ and $\mathbf{u}$ is not known, it is estimated as,

$$\dot{\mathbf{x}} = \hat{\mathbf{J}}\dot{\mathbf{u}} \qquad (16)$$

By combining (15) and (16) we obtain:

$$\dot{\mathbf{u}} = -\lambda\hat{\mathbf{J}}^+(\mathbf{x} - \mathbf{x}_{des}) \qquad (17)$$

with $\hat{\mathbf{J}}^+$ being the Moore–Penrose inverse of the estimated sensitivity Jacobian matrix $\hat{\mathbf{J}}$. From (6), $\mathbf{J}$ is a function of $\mathbf{u}$. It means that several estimated matrix $\hat{\mathbf{J}}$ can be found. Here, the used estimated sensitivity matrix named $\hat{\mathbf{J}}_*$ is the matrix $\mathbf{J}$ assessed at the final desired configuration $\mathbf{u}^d$ of the beam, i.e., for $y_d = 0.8$ m and $z_d = 0$ m. It will be shown in Sec. 4.2 that this choice is relevant in terms of control stability. As a result, the control law is:

$$\dot{\mathbf{u}} = -\lambda\hat{\mathbf{J}}_*^+(\mathbf{x} - \mathbf{x}_{des}) \qquad (18)$$

Note that (18) provides a velocity in $\mathcal{DIS}$ whereas the control law requires the variation $\delta\mathbf{u}$. As a consequence, a duration t_u of motion is defined and the control law becomes:

$$\delta\mathbf{u} = -\lambda t_u\hat{\mathbf{J}}_*^+(\mathbf{x} - \mathbf{x}_{des}) \qquad (19)$$

Note that t_u is about twenty times the sampling period, the latter equals 5 ms, of the low level control of the KUKA LWR 4+ robotic arms.

4.1 Stability Analysis

The stability analysis is useful to understand at first glance the performance of the control law. First, a Lyapunov function $\mathbb{L}$ based on the tracking error is defined to study the stability:

$$\mathbb{L} = \frac{1}{2}\mathbf{e}^T\mathbf{e} \qquad (20)$$

The derivative of $\mathbb{L}$ is:

$$\dot{\mathbb{L}} = \mathbf{e}^T\dot{\mathbf{e}} \qquad (21)$$

Since the desired position and shape of the beam are fixed, the evolution of the error $\dot{\mathbf{e}}$ as function of the control input can be expressed as:

$$\dot{\mathbf{e}} = \dot{\mathbf{x}} = \mathbf{J}(\mathbf{u})\dot{\mathbf{u}} \qquad (22)$$

With the proposed control law (18), $\dot{\mathbf{e}}$ takes the form:

$$\dot{\mathbf{e}} = -\lambda\mathbf{J}(\mathbf{u})\hat{\mathbf{J}}_*^+\mathbf{e} \qquad (23)$$

Using (23) in (21), we obtain

$$\dot{\mathbb{L}} = -\lambda\mathbf{e}^T\mathbf{J}(\mathbf{u})\hat{\mathbf{J}}_*^+\mathbf{e} \qquad (24)$$

If the matrix $\mathbf{J}(\mathbf{u})\hat{\mathbf{J}}_*^+$ is positive definite, the convergence of $\mathbf{e}$ to zero will be insured. However this matrix is a $(2N \times 2N)$-matrix of rank ≤ 4. Thus this condition cannot be met when $N > 2$.

It should be noted that if $\hat{\mathbf{J}}_*^+\mathbf{e} = 0$, i.e., if $\mathbf{x} - \mathbf{x}_{des}$ is in the kernel of $\hat{\mathbf{J}}_*^+$, then the $\dot{\mathbf{u}}$ command will be null and the error $\mathbf{e}$ will not be reduced but will remain constant. Knowing that the final error cannot always be null since $N \geq 3$ control points are used for four available commands only, the evolution of the error projected in the image of $\hat{\mathbf{J}}_*^+$ is studied. Accordingly, a new four-dimensional error vector ϵ is defined as follows:

$$\epsilon = \hat{\mathbf{J}}_*^+\mathbf{e} \qquad (25)$$

The evolution of ϵ can be deduced by time derivation of (25), namely,

$$\dot{\epsilon} = \hat{\mathbf{J}}_*^+\dot{\mathbf{e}} \qquad (26)$$

since $\hat{\mathbf{J}}_*^+$ is a constant matrix. Using (23), and (25), $\dot{\epsilon}$ can be expressed as:

$$\dot{\epsilon} = -\lambda\hat{\mathbf{J}}_*^+\mathbf{J}(\mathbf{u})\epsilon \qquad (27)$$

From (27), a sufficient condition to ensure the system stability is the matrix $\hat{\mathbf{J}}_*^+\mathbf{J}(\mathbf{u})$ to be positive definite (Zake *et al.* (2019a); Zake *et al.* (2019b)). Since $\hat{\mathbf{J}}_*^+\mathbf{J}(\mathbf{u})$ may not be symmetric, its definite positiveness is analyzed based on the eigenvalues of its associated symmetric matrix $\blacksquare$. As a result, a sufficient condition to ensure the system stability becomes:

$$\blacksquare = 1/2(\hat{\mathbf{J}}_*^+\mathbf{J}(\mathbf{u}))^T + 1/2(\hat{\mathbf{J}}_*^+\mathbf{J}(\mathbf{u})) > \mathbf{0}, \forall t \qquad (28)$$

Indeed, if this condition is satisfied, the error $\dot{\epsilon}$ will always decrease to finally reach $\mathbf{0}$. The results on local stability of the proposed control law are given in Sec. 4.2.

As far as the final error is concerned, if the position $\mathbf{x}_{des}$ of the target markers and the position $\mathbf{x}$ of the markers stuck the beam are such that moving one of the robot end-effectors to reduce a distance for one marker to its target leads to an increase of a distance from another marker to its own target, the controller will have better do nothing. From (6), only the error $\mathbf{x} - \mathbf{x}_{des}$ that belongs to the image of $\mathbf{J}$ can be reduced by the control input. The part of the error that is in the kernel of $\mathbf{J}(\mathbf{u})^+$ cannot be cancelled. Since the proposed control law is built based on sensitivity matrix $\mathbf{J}$ estimated at the expected final pose and shape of the beam, it leads to the smallest final error.

4.2 Simulation

The aforementioned method can be implemented by means of Simscape Multibody$^{\text{TM}}$ and Simulink$^{\text{TM}}$. The control law minimizes the error between each keypoint on the beam and its assigned marker on the target shape as shown in Fig. 11 while considering large position errors for the keypoints at the start configuration.

Figure 12 shows that the four eigenvalues of matrix $\blacksquare$ are positive within the intervals $0.8\ \text{m} < y_d < 1\ \text{m}$ and $-0.2\ \text{m} < z_d < 0\ \text{m}$. From (28), the system will be stable for any initial configuration (y_{d0}, z_{d0}) taken in those intervals with the final configuration $(y_{df}, z_{df}) = (0.8\ \text{m}, 0\ \text{m})$.

In addition to stability analysis, the error ξ in $\mathcal{KS}$ is considered as another performance index of control law (18). ξ is the root-mean square error of the keypoint position:

$$\xi = \sqrt{||\mathbf{x} - \mathbf{x}_{des}||^2} / N \qquad (29)$$

Figure 13(a) shows the evolution of ξ with time for the simulated system, $N = 3$. ξ decreases and stabilizes at a small value as expected.
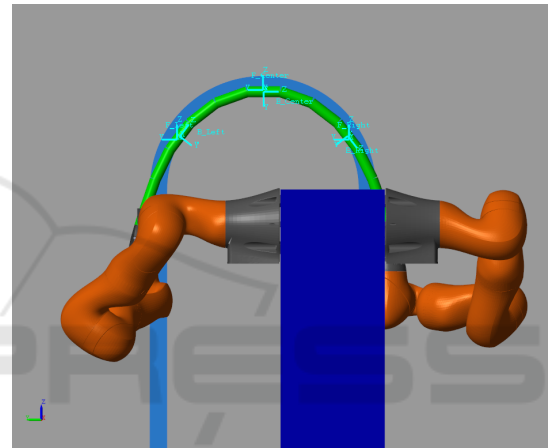
4.3 Experiments

Figure 14 and video[2] represent the task performed experimentally thanks to control law (18). The corresponding values of ξ defined in (29) are depicted in Fig. 13b. The experimental decrease of ξ is slower than the simulated one because of the slow detection of the ArUco markers by the low-cost camera used and vibrations.

[2]https://uncloud.univ-nantes.fr/index.php/s/kZpNNAQ98PpBr9C
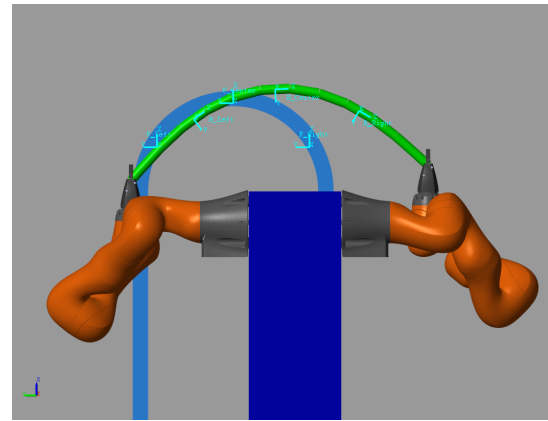
(a)

(b)

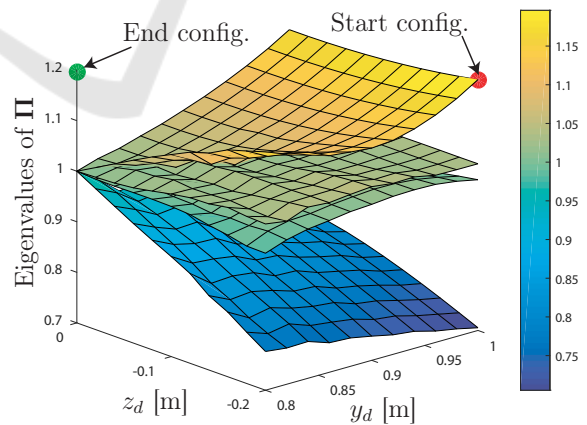Figure 11: Start (a) and end (b) of the task in simulation.

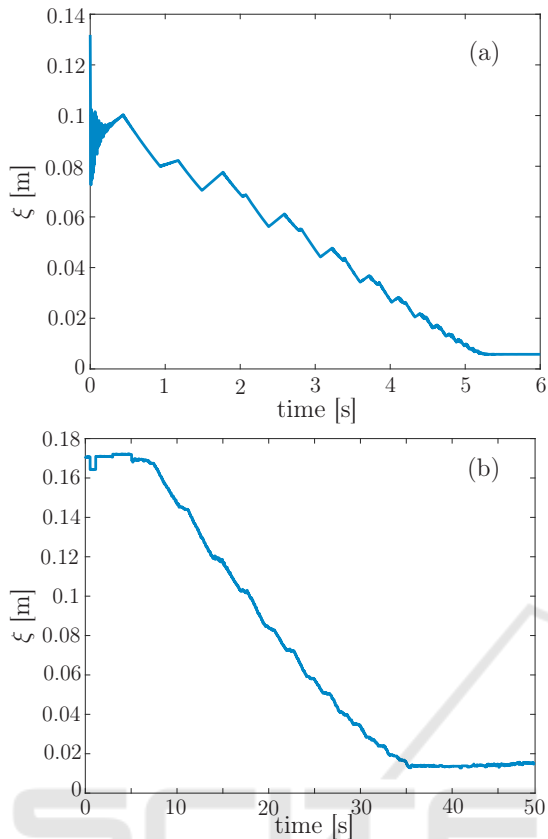Figure 12: The eigenvalues of $\blacksquare$ as a function of y_d and z_d.

Figure 13: Root-mean square error of the keypoint position: (a) simulation; (b) experiments.

Figure 14: Start (a) and end (b) of the task experimentally.

5 CONCLUSIONS AND FUTURE WORK

This paper dealt with a control law for manipulating a flexible beam with a dual-arm robot. The approach is characterized by the fact that a deformation model of the object is not necessary since it is experimentally constructed. This will be particularly useful if the material is anisotropic or poorly identified. The built model is adapted to the proposed control law because the elastic deformations induced by the beam deformation provided by the robots are measured. A fairly complete simulation study showed that it is possible to only use the deformation model of the flexible object corresponding to its intended configuration for manipulation by ensuring the stability of the control through the whole task. Accordingly, an online estimation as proposed in (Navarro-Alarcon *et al.* (2016)) is not required with the control approach presented in this paper. Indeed an acceptable deformation model of the beam is constructed experimentally. The contribution of the paper is essentially methodological and the results are illustrated with the planar deformation
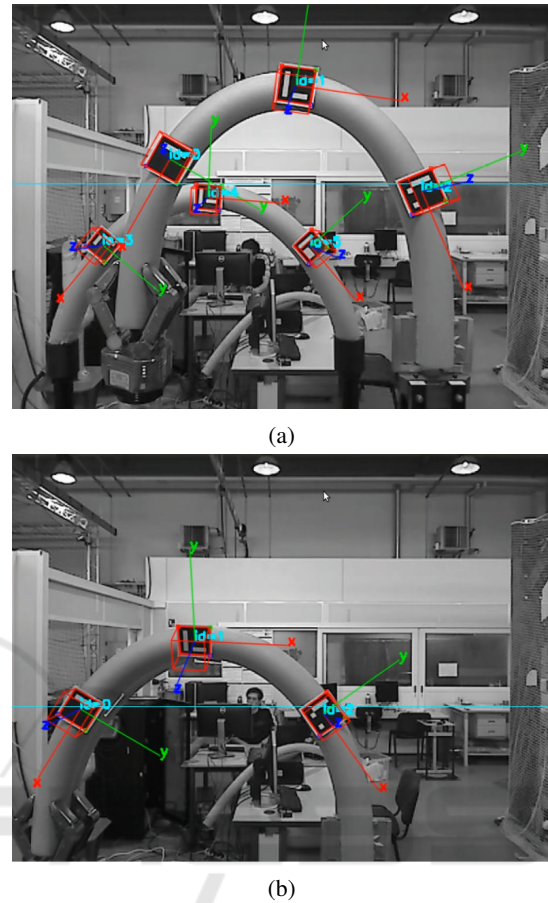
of a beam using markers. Later on, the proposed approach will be extended to the positioning, shaping and assembling of three-dimensional flexible objects with more than two robotic arms. The online detection of the beam deformation was performed thanks to some markers as a proof of concept. Such a detection can be extended by using points of interest extracted from images.

REFERENCES

J. Marvel, R. Bostelman, and J. Falco, Multi-Robot Assembly Strategies and Metrics, ACM Comput Surv., vol. 51(1), 2018. doi: 10.1145/3150225.

D. Sun, Y.H. Liu, Modeling and impedance control of a two-manipulator system handling a flexible beam, ASME J. Dyn. Syst. Meas. Control, vol. 119, no. 4, pp. 736-742, Dec. 1997.

S. Erhart, and S. Hirche, Adaptive force/velocity control for multi-robot cooperative manipulation under uncertain kinematic parameters, Proceedings of the IEEE/RSJ International Conference on Intelligent

Robots and Systems, pp. 307-314, Nov. 2013, doi: 10.1109/IROS.2013.6696369.

D. Sun, Y.H. Liu, Position and force tracking of a two-manipulator system manipulating a flexible beam, J. Robot. Syst., vol. 18, no. 4, pp. 197-212, March 2001.

S. Hirai, T. Wada, Indirect simultaneous positioning of deformable objects with multi-pinching fingers based on an uncertain model, Robotica, vol. 18, no. 1, pp. 3–11, Jan. 2000, doi: 10.1017/S0263574799002362.

A. Tavasoli, M. Eghtesad, and H. Jafarian, Two-time scale control and observer design for trajectory tracking of two cooperating robot manipulators moving a fexible beam, Robotics and Autonomous Systems, vol. 57, no. 2, pp. 212 - 221, 2009, https://doi.org/10.1016/j.robot.2008.04.003.

J. Smolen and A. Patriciu, Deformation Planning for Robotic Soft Tissue Manipulation, in 2009 Second International Conferences on Advances in Computer-Human Interactions, pp. 199–204, Feb. 2009.

T. Wada, S. Hirai, S. Kawarnura, and N. Karniji, Robust manipulation of deformable objects by a simple PID feedback, in Proc. IEEE International Conference on Robotics and Automation (ICRA), pp. 85–90, 2001.

D. Navarro-Alarcon et al., Automatic 3-D Manipulation of Soft Objects by Robotic Arms With an Adaptive Deformation Model, in IEEE Transactions on Robotics, vol. 32, no. 2, pp. 429-441, April 2016, doi : 10.1109/TRO.2016.2533639

D. Berenson, Manipulation of deformable objects without modeling and simulating deformation, 2013 IEEE/RSJ International Conference on Intelligent Robots and Systems, Tokyo, pp. 4525-4532, 2013. doi: 10.1109/IROS.2013.6697007.

B. Jia, Z. Hu, J. Pan and D. Manocha, Manipulating Highly Deformable Materials Using a Visual Feedback Dictionary, 2018 IEEE International Conference on Robotics and Automation (ICRA), Brisbane, QLD, pp. 239-246, 2018. doi: 10.1109/ICRA.2018.8461264

F. Bertelsmeier, T. Detert, T. Übelhör, R. Schmitt and B. Corves, Cooperating Robot Force Control for Positioning and Untwisting of Thin Walled Components, Advances in Robotics and Automation, vol. 3, no. 6, Nov. 2017, doi: 10.4172/2168-9695.1000179.

A.S. Al-Yahmadi, and T.C. Hsia, Modeling and Control of Two Manipulators handling a Flexible Beam, International Journal of Electrical and Computer Engineering, vol. 1, no. 6, pp. 934-937, Nov. 2007.

S. Garrido-Jurado, R. Muñoz-Salinas, F.J. Madrid-Cuevas, and M.J. Marìn-Jiménez. 2014. Automatic generation and detection of highly reliable fiducial markers under occlusion. Pattern Recogn. vol. 47, no. 6, pp. 2280-2292, June 2014. DOI=10.1016/j.patcog.2014.01.005

S. Caro, N. Binaud, and P. Wenger, Sensitivity Analysis of 3-RPR Planar Parallel Manipulators, ASME Journal of Mechanical Design, vol. 131, pp. 121005-1–121005-13, 2009.

S. Miller et al., Technical Paper at Mathworks, Modeling Flexible Bodies with Simscape Multibody Software, 2006.

F. Chaumette, P. Rives, and B. Espiau, Positioning of a robot with respect to an object, tracking it and estimating its velocity by visual servoing, Proceedings. 1991 IEEE International Conference on Robotics and Automation, Sacramento, CA, USA, vol. 3, pp. 2248-2253, 1991.

Z. Zake, F. Chaumette, N. Pedemonte, and S. Caro, Vision-Based Control and Stability Analysis of a Cable-Driven Parallel Robot, in the IEEE Robotics and Automation Letters (RA-L), vol. 4, no. 2, pp. 1029-1036, 2019

Z. Zake, S. Caro, A.S. Roos, F. Chaumette and N. Pedemonte, Stability Analysis of Pose-Based Visual Servoing Control of Cable-Driven Parallel Robots. In: Pott A., Bruckmann T. (eds) Cable-Driven Parallel Robots. CableCon 2019. Mechanisms and Machine Science, vol. 74. Springer, Cham.

A. Sintov, S. Macenski, A. Borum, T. Bretl, Motion Planning for Dual-Arm Manipulation of Elastic Rods. IEEE Robotics and Automation Letters, vol. 5, N° 4, October 2020.

T. Bretl, Z. McCarthy, "Quasi-static manipulation of a Kirchhoff elastic rod based on a geometric analysis of equilibrium configurations", Int. J. Robot. Res., vol. 33, no. 1, pp. 48-68, 2014.

R. Lagneau, A. Krupa and M. Marchal, Automatic Shape Control of Deformable Wires based on Model-Free Visual Servoing. IEEE Robotics and Automation Letters, IEEE 2020, 5 (4), pp. 5252-5259. 10.1109/LRA.2020.3007114